



## Estimation and Optimization of the Radiant Field in Flat Plate Heterogeneous Photoreactors with the P1-approximation of the Radiative Transfer Equation (RTE)

Clovis Nchikou 

Universidad Autónoma de Nuevo León, Facultad de Ciencias Químicas, San Nicolás De Los Garza, 6645, México.

**Abstract:** In this work, the P1-approximation of the radiative transfer equation (RTE) was used for the description and optimization of the radiant field in a flat plate photoreactor under solar radiation with three commercial brands of titanium dioxide photocatalysts. The boundary layer of photon absorption ( $[\delta_{\text{abs}}]$ ), the average volumetric rate of photon absorption ( $V_{\text{RPA}}$ ), and a new apparent optical thickness ( $\zeta_{\text{app1}}$ ) were used as design parameters for optimization. A simple mathematical expression for the calculation of  $\delta_{\text{abs}}$  also called the best reactor thickness was formulated. For the three catalysts, varying the reactor height ( $L$ ) resulted in a decrease in the local volumetric rate of photon absorption ( $L_{\text{VRPA}}$ ) from the top side to the bottom of the reactor for any value of the catalyst loading ( $C_{\text{cat}}$ ). It was also observed that when  $C_{\text{cat}}$  increases the  $V_{\text{RPA}}$  increases exponentially until a fixed value where it remains almost constant. With  $L = 1$  cm, the optimum  $C_{\text{cat}}$  ( $C_{\text{cat-op}}$ ) was 0.2 g/L in 0.85 cm of thickness, 0.3 g/L in 0.82 cm of thickness, and 0.4 g/L in 0.89 cm of thickness for the photocatalysts Catalyst D P-25, Catalyst A, and Catalyst H, respectively. The optimum apparent optical thickness ( $\zeta_{\text{app1,op}}$ ) was 4.87, 4.62, and 3.7 for the photocatalysts Catalyst D P-25, Catalyst A, and Catalyst H, respectively. These results are in good agreement with the literature. Results found in this work give predictions on radiation absorption in flat plate photocatalytic reactors with different heights.

**Keywords:** Flat plate reactor, Boundary layer,  $L_{\text{VRPA}}$ , Titanium dioxide, P1-approximation.

**Submitted:** March 12, 2024. **Accepted:** May 04, 2024.

**Cite this:** Nchikou, C. (2024). Estimation and Optimization of the Radiant Field in Flat Plate Heterogeneous Photoreactors with the P1-approximation of the Radiative Transfer Equation (RTE). *Journal of the Turkish Chemical Society, Section B: Chemical Engineering*, 7(1), 87–104. <https://doi.org/10.58692/jotcsb.1450662>

**Corresponding author. E-mail:** [clovis.nchikou@uanl.edu.mx](mailto:clovis.nchikou@uanl.edu.mx).

## 1. INTRODUCTION

Water pollution is one of the major global issues, primarily affecting developing countries. Several approaches have been put out to address this situation. For many decades now, heterogeneous photocatalysis has been considered a potential oxidation method for disinfecting and decontaminating water (He et al., 2021; Li et al., 2022; Nair & Jagadeesh Babu, 2017). It is an advanced oxidation technology based on the photo-excitation of photocatalysts with solar or artificial radiation. The activation of a semiconductor with an energy equal to or greater than its band gap energy generates electron-hole pairs, which in contact with charge carriers ( $H_2O$ ,  $OH^-$ ,  $O_2$ , etc) produce radical oxidative species such as hydroxyl radicals. These radicals are transitory compounds that attack contaminants present in the fluid phase through oxidative or reductive reaction pathways (Li Puma et al., 2020). Research on solar photocatalysis as a clean technology for producing hydrogen and solar fuels, as well as a sustainable alternative to treating industrial wastewater and removing organic pollutants, dyes, pesticides, and emerging contaminants, has increased dramatically as a result of the ongoing concern

about water remediation (Rizzo et al., 2019; Vaya & Surolia, 2020). Because mathematical modeling is crucial to the design, assessment, optimization, and efficiency estimation of photoreactors at various sizes, it has become more and more relevant in this field (Wang et al., 2021). The mathematical modeling of photocatalysis processes is composed of a sequence of sub-models including the modeling of the radiant field (Ochoa-Gutiérrez et al., 2018). This sub-model includes the solar emission model and the absorption-scattering model for the quantification of the *LVRPA*, one of the key parameters of the intrinsic kinetic equation (Colina-Márquez et al., 2015). The *LVRPA* depends on the geometry, radiation source, catalyst loading, and type of photocatalyst, in some cases on the pollutant if this presents absorption of radiant energy. For its determination, one should solve the RTE which remains a challenging task due to its integro-differential form (Illi et al., 2019). Eq. (1) traduces the steady-state and non-temperature-dependence of the RTE, which describes the different phenomena that occur on the light when it traverses a medium, such as absorption, in-scattering, and out-scattering as represented in Eq. (1).

$$\frac{dI_\lambda(S, \Omega)}{ds} = -K I_\lambda(S, \Omega) - \sigma_\lambda I_\lambda(S, \Omega) + \frac{\sigma_\lambda}{4\pi} \int_{\Omega=4\pi} P(\Omega' \rightarrow \Omega) I_\lambda(S, \Omega') d\Omega' \quad (1)$$

where  $I_\lambda$  is the photon irradiance ( $W/m^2$ ),  $K_\lambda$  the absorption coefficient ( $m^2/kg$ ),  $\sigma_\lambda$  the scattering coefficient ( $m^2/kg$ ),  $P(\Omega' \rightarrow \Omega)$  the scattering phase function,  $\lambda$  the wavelength (m),  $S$  the spatial coordinate (m) and  $\Omega$  the directional solid angle (Steradian) (Fujii et al., 2022; Ghafoori et al., 2020; Howell et al., 2021).

The RTE gives an account of how light is dispersed or absorbed within a specific medium. Numerous numerical techniques, such as the discrete ordinate methods (DOM) and the Monte Carlo model, were employed to solve the RTE; nevertheless, these methods are time-consuming and need significant processing resources (Acosta-Herazo et al., 2020; Moreno-SanSegundo et al., 2020; Peralta Muniz Moreira & Li Puma,

2021). Alternative analytic methods such as the n-flux or the Pn approximation models (n is a strictly positive integer) have been used to solve the RTE, to describe and quantify satisfactorily the radiant field in various types of photocatalytic reactors (Arancibia-Bulnes et al., 2009; Cuevas et al., 2007). The P1-approximation is the lowest order of the spherical harmonics method (also known as the Pn-approximation), i.e., keeps only the first two terms of the Pn-approximation (Akdemir et al., 2022; Christenson et al., 2018; Harel et al., 2021). It is more versatile than two and four-flux models because it lends itself more easily to different geometries (Arancibia-Bulnes et al., 2009). It has been used to solve the RTE in one dimension in flat plate photoreactors and two dimensions in cylindrical photoreactors (Arancibia-Bulnes et al., 2009; Cuevas & Arancibia-Bulnes, s. f.). The P1 approximation

saves computational time and effort by reducing the mathematical complexity of the RTE to an analytical equation (Arancibia-Bulnes et al., 2009; Cuevas et al., 2007; Cuevas & Arancibia-Bulnes, s. f.). Flat plate reactors can be scaled up and can be used with solar radiation, so they are very attractive and also provide an excellent configuration for efficient activation of the photocatalyst TiO<sub>2</sub> (Li Puma, 2005). Their modeling requires a complex analysis of the radiation field inside the photoreactor (Cassano et al., 1995).

In this paper, the P1 approximation was used to model radiant fields and to find the optimum operational conditions in flat plate heterogeneous photoreactors under solar radiation. Three commercial brands of titanium dioxide photocatalysts (Catalyst D, Catalyst A, and Catalyst H) were used and some comparisons were made between them. Design parameters such as the *VRPA*, the best reactor thickness  $\delta_{abs}$ , and a new apparent optical thickness  $\zeta_{app1}$  were used.  $\zeta_{app1}$  was formulated with the P1 approximation approach. Kinetic models of pollution degradation and hydrogen production could benefit from the information provided. In kinetic models of pollution degradation and hydrogen production, determining the local volumetric rate of photon absorption might help to improve understanding of the relevant processes. It makes it possible to calculate reaction rates, energy transfer, and overall efficiency precisely, which improves environmental results and leads to optimal systems.

## 2. MATERIALS AND METHODS

### 2. 1. Radiant field

The radiant field was estimated by solving the RTE in one dimension in rectangular coordinates, and then the *LVRPA* was deduced. Eq. (2) is the governing equation of the P1 approximation or the so-called Helmholtz's equation which will be solved later in one dimension with suitable boundary conditions.

$$\Delta G_{\lambda} = k_{d,\lambda}^2 G_{\lambda} \quad (2)$$

where,

$$k_{d,\lambda} = \beta_{\lambda} \sqrt{3(1-\omega_{\lambda})(1-g_{\lambda} \frac{\omega_{\lambda}}{3})} \quad (3)$$

where  $g_{\lambda}$  is the asymmetry Henyey-Greenstein phase function factor corresponding to the monochromatic radiation of wavelength  $\lambda$  and which is proper to each catalyst,  $\beta_{\lambda}$  is the monochromatic extinction coefficient being the sum of  $\kappa_{\lambda}$  and  $\sigma_{\lambda}$  which are the monochromatic absorption and scattering coefficients respectively defined as,

$$\beta_{\lambda} = \kappa_{\lambda} + \sigma_{\lambda} \quad (4)$$

All of these coefficients depend on catalyst particle concentration in a linear fashion as,

$$\beta_{\lambda} = \beta_{\lambda}^* C_{cat}, \kappa_{\lambda} = \kappa_{\lambda}^* C_{cat}, \sigma_{\lambda} = \sigma_{\lambda}^* C_{cat} \quad (5)$$

where  $C_{cat}$  is the catalyst concentration,  $\beta_{\lambda}^*$ ,  $\kappa_{\lambda}^*$  and  $\sigma_{\lambda}^*$  are specific coefficients, independent of this concentration (for values in the usual ranges for photocatalysis).

$\omega_{\lambda}$  is the scattering albedo which gives the probability that a photon is scattered when colliding with a particle defined as,

$$\omega_{\lambda} = \frac{\sigma_{\lambda}}{\beta_{\lambda}} \quad (6)$$

Instead of using the monochromatic parameters, one should use their average values in a defined wavelength interval  $[\lambda_{min}, \lambda_{max}]$  using the following equation,

$$\Gamma^* = \frac{\int_{\lambda_{min}}^{\lambda_{max}} \Gamma_{\lambda} I(\lambda) d\lambda}{\int_{\lambda_{min}}^{\lambda_{max}} I(\lambda) d\lambda} \quad (7)$$

where  $\Gamma_{\lambda}$  can be one of the parameters  $\kappa_{\lambda}$ ,  $\sigma_{\lambda}$ ,  $\beta_{\lambda}$  or  $g_{\lambda}$  and  $\lambda_{min} = 280$  nm,  $\lambda_{max} = 395$  nm given by the interception of solar emission spectrum and titanium dioxide absorption spectrum;  $I(\lambda)$  is the spectrum of solar emission power (Tourasse & Dumortier, 2014).

$G_\lambda$  is the local radiation which corresponds to the integration of the irradiance  $I_\lambda$  all over the solid angle  $\Omega$ . After finding the expression of  $G_\lambda$ , one can easily deduce the local volumetric rate of photon absorption (LVRPA) from Eq. (8); this parameter is very important for the determination of the intrinsic kinetic rate of the photocatalytic reaction in a given reaction system.

$$LVRPA = k_\lambda G_\lambda \quad (8)$$

In this paper, the concept of the boundary layer of photon absorption introduced yet in the literature (Otálvaro-Marín et al., 2014) and which allows the determination of the best thickness has been discussed with the P1 approximation approach. Figure 1 represents a flat plate reactor with thickness  $L$ , located perpendicularly to the

source, where  $I_0$  represents the constant incident radiation intensity. The region where there is a gradient of energy absorption has been called the boundary layer of photon absorption, and its thickness  $\delta_{abs}$  which can be understood as the reactor thickness measured from the irradiated surface where 99% of total energy is absorbed. Then  $\delta_{abs}$  is defined as  $x$ -value which satisfies the following equation:

$$\int_0^{\delta_{abs}} LVRPA(x) dx = 0.99 \int_0^L LVRPA(x) dx \quad (9)$$

This definition of boundary layer thickness for transport phenomena and absorption of radiant energy is analogous to the definition of thickness of hydrodynamic, thermal, and concentration boundary layer on a flat plate (Incropera, s. f.; Otálvaro-Marín et al., 2014).

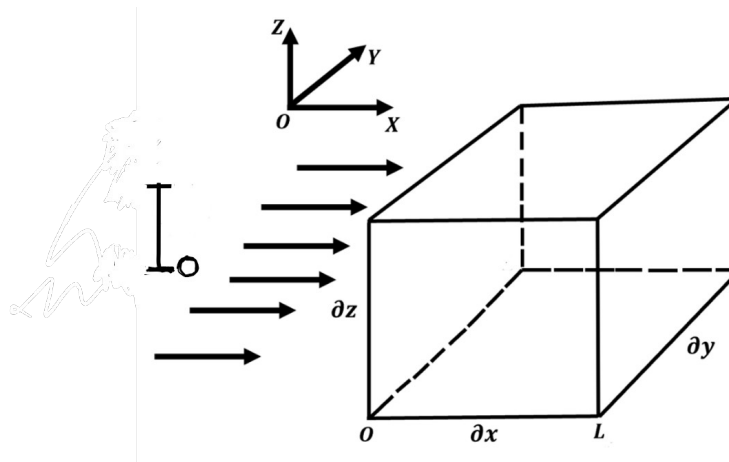


Figure 1. Collimated incident radiation on a slab reactor.

Oversizing the reactor thickness could lead to the formation of a dark sublayer with very little photon absorption. As a result, while choosing the ideal thickness for flat plate reactors, the boundary layer thickness becomes a design parameter (Otálvaro-Marín et al., 2014). It can be used as a geometrical parameter that is equivalent to the optimal reactor thickness, depending on the type and loading of the catalyst. It is worth mentioning that the new apparent optical thickness was also formulated

here with the P1 approximation approach and was used for a design purpose.

## 2. 2. Solution for the RTE in One Dimension Using the P1 Approximation Approach

Figure 1 shows a schematic representation of a flat plate reactor with thickness  $L$ , located perpendicularly to the source.

The P1 approximation in one dimension in cartesian coordinates becomes:

$$\frac{\partial G_\lambda}{\partial x} = k_{d,\lambda}^2 G_\lambda \tag{10}$$

$$\xi_\lambda = \beta_\lambda \left(1 - g_\lambda \frac{\omega}{3}\right) \tag{14}$$

The general solution of Eq. 10 is:

$$G_\lambda = A e^{k_{d,\lambda} x} + B e^{-k_{d,\lambda} x} \tag{11}$$

where  $A$  and  $B$  are real constants to determine later.

**2. 3. Boundary Conditions**

For the determination of the constants  $A$  and  $B$  Marshak’s boundary conditions (Marshak, 1947) are considered in Eqs. (1-2), where  $I_0$  represents the photon flux reaching perpendicularly the top side of the reactor and with the assumption that the photon flux does not reach the reactor bottom and that the inner reflectance of reactor glass is negligible.

$$G_\lambda(0) - \frac{2}{3\xi_\lambda} \frac{dG_\lambda(x)}{dx} \Big|_{x=0} = 4I_0 \tag{12}$$

$$G_\lambda(L) + \frac{2}{3\xi_\lambda} \frac{dG_\lambda(x)}{dx} \Big|_{x=L} = 0 \tag{13}$$

where ,

That leads to the following system of equations:

$$\left(1 - \frac{2k_{d,\lambda}}{3\xi_\lambda}\right) A + \left(1 + \frac{2k_{d,\lambda}}{3\xi_\lambda}\right) B = 4I_0 \tag{15}$$

$$\left(1 + \frac{2k_{d,\lambda}}{3\xi_\lambda}\right) e^{k_{d,\lambda} L} A + \left(1 - \frac{2k_{d,\lambda}}{3\xi_\lambda}\right) e^{-k_{d,\lambda} L} B = 0 \tag{16}$$

Which yields

$$A = \frac{4\left(1 - \frac{2k_{d,\lambda}}{3\xi_\lambda}\right) e^{-k_{d,\lambda} L} I_0}{\left(1 - \frac{2k_{d,\lambda}}{3\xi_\lambda}\right)^2 e^{-k_{d,\lambda} L} - \left(1 + \frac{2k_{d,\lambda}}{3\xi_\lambda}\right)^2 e^{k_{d,\lambda} L}} \tag{17}$$

$$B = \frac{-4\left(1 + \frac{2k_{d,\lambda}}{3\xi_\lambda}\right) e^{k_{d,\lambda} L} I_0}{\left(1 - \frac{2k_{d,\lambda}}{3\xi_\lambda}\right)^2 e^{-k_{d,\lambda} L} - \left(1 + \frac{2k_{d,\lambda}}{3\xi_\lambda}\right)^2 e^{k_{d,\lambda} L}} \tag{18}$$

Finally, one finds,

$$G_\lambda(x) = \frac{4\left(1 - \frac{2k_{d,\lambda}}{3\xi_\lambda}\right) e^{-k_{d,\lambda}(L-x)} - 4\left(1 + \frac{2k_{d,\lambda}}{3\xi_\lambda}\right) e^{k_{d,\lambda}(L-x)}}{\left(1 - \frac{2k_{d,\lambda}}{3\xi_\lambda}\right)^2 e^{-k_{d,\lambda} L} - \left(1 + \frac{2k_{d,\lambda}}{3\xi_\lambda}\right)^2 e^{k_{d,\lambda} L}} I_0 \tag{19}$$

The local volumetric rate of photon absorption will be then,

$$LVRPA(x) = \frac{4\kappa_\lambda \left( \left(1 - \frac{2k_{d,\lambda}}{3\xi_\lambda}\right) e^{-k_{d,\lambda}(L-x)} - \left(1 + \frac{2k_{d,\lambda}}{3\xi_\lambda}\right) e^{k_{d,\lambda}(L-x)} \right)}{\left(1 - \frac{2k_{d,\lambda}}{3\xi_\lambda}\right)^2 e^{-k_{d,\lambda}L} - \left(1 + \frac{2k_{d,\lambda}}{3\xi_\lambda}\right)^2 e^{k_{d,\lambda}L}} I_0 \quad (20)$$

**2. 4. Parameters of the P1 Approximation**

$\omega_{\lambda,mod}$ ,  $\lambda_{mod}$  and  $\zeta_{app1}$  are defined here as the P1 approximation parameters, their equivalent are  $\omega_{corr}$ ,  $\lambda_{corr}$  and  $\zeta_{app}$  for the six-flux model (SFM) respectively,  $\zeta_{app1}$  is a design parameter as  $\zeta_{app}$  is for the SFM (*mod* stands for *modified*). These parameters are defined as follows:

$$\lambda_0 = \frac{1}{\beta_\lambda} \quad (23)$$

$\zeta_{app1}$  is the apparent optimal thickness defined as

$$\omega_{\lambda,mod} = \sqrt{\omega_\lambda \left(1 + \frac{g_\lambda}{3} - \frac{g_\lambda}{3} \omega_\lambda\right)} \quad (21)$$

$$\zeta_{app1} = \zeta \sqrt{3(1 - \omega_{\lambda,mod}^2)} \quad (24)$$

where  $\zeta$  is the optical thickness, for a flat plate reactor expressed as,

$$\lambda_{mod} = \frac{\lambda_0}{\sqrt{3(1 - \omega_{\lambda,mod}^2)}} \quad (22)$$

$$\zeta = \frac{L}{\lambda_0} \quad (25)$$

where  $\lambda_0$  is the mean free path of photon defined as,

$$k_{d,\lambda} = \frac{1}{\lambda_{mod}} \quad (26)$$

$$LVRPA(x) = \frac{4\kappa_\lambda \left( \left(1 - \frac{2}{3\xi_\lambda}\right) e^{\frac{-L-x}{\lambda_{mod}}} - \left(1 + \frac{2}{3\xi_\lambda}\right) e^{\frac{L-x}{\lambda_{mod}}} \right)}{\left(1 - \frac{2}{3\xi_\lambda}\right)^2 e^{\frac{-L}{\lambda_{mod}}} - \left(1 + \frac{2}{3\xi_\lambda}\right)^2 e^{\frac{L}{\lambda_{mod}}}} I_0 \quad (27)$$

The unique solution for Eq. (9) is given by:

where,

$$\delta_{abs} = \lambda_{mod} \ln\left(\frac{\Sigma + \sqrt{\Sigma^2 + 4AB}}{2A}\right) \quad (28)$$

$$\Sigma = 0.99(A e^{\frac{L}{\lambda_{mod}}} - B e^{\frac{-L}{\lambda_{mod}}} - A + B) + A - B \quad (29)$$

where  $A$  and  $B$  are constants defined in Eqs. (17-18) respectively.

## 2. 5. Volumetric Rate of Photon Absorption, $VRPA$

$VRPA$  is defined as an average value of  $LVRPA$  in the entire reactor volume. For a flat plate reactor, when the incident radiation intensity is constant along the reactor wall, the is expressed as:

$$VRPA = \frac{1}{L} \int_0^L LVRPA(x, C_{cat}) dx \quad (30)$$

$VRPA$  is a design parameter formulated and validated to determine the optimum catalyst loadings in photocatalytic processes (Brandi et al., 1996; Otálvaro-Marín et al., 2014).

## 3. RESULTS AND DISCUSSION

The simulation of the P1 approximation in a flat plate photoreactor was performed under solar radiation with three different brands of commercial titanium dioxide with their optical characteristics (albedo, modified albedo, scattering and absorption coefficient, asymmetry factor) reported in the literature (Acosta-Herazo et al., 2016; Otálvaro-Marín et al., 2014) and in Table 1. The reactor thickness  $L$  was considered to vary.

**Table 1.** Average optical properties of commercial photocatalysts based on titanium dioxide under solar radiation (Acosta-Herazo et al., 2016; Otálvaro-Marín et al., 2014), modified albedo, and asymmetry factor  $g$ .

Catalyst	$\sigma^* \times 10^{-4}$ ( $cm^2 g^{-1}$ )	$\kappa^* \times 10^{-3}$ ( $cm^2 g^{-1}$ )	$\beta^* \times 10^{-4}$ ( $cm^2 g^{-1}$ )	$\omega$	$\omega_{mod}$	$g$
Catalyst A	3.73	2.43	3.98	0.94	0.97	0.53
Catalyst D	5.42	2.87	5.71	0.95	0.99	0.53
Catalyst H	2.52	1.17	2.64	0.96	0.98	0.57

### 3.1. $LVRPA$

The local volumetric rate of photon absorption per unit of incoming radiant flux ( $LVRPA/I_0$ ) in function of x-coordinate at different catalyst loads describes the distribution of the photon absorption inside the reactor for each of the catalysts Catalyst A, Catalyst D and Catalyst H as depicted in Figure 2 ( $L=1$  cm). For each catalyst, the  $LVRPA/I_0$  profile shows the decrease of the absorption from the top side (Maximum value of  $LVRPA/I_0$ ) until the bottom of the reactor (minimum value of  $LVRPA/I_0$ ) and that the absorption at the top side of the reactor increases exponentially with the increase of the

catalyst load due to the amount of surface-exposed catalyst and the back-scattering energy absorption from the internal layer inside the reactor. Near the irradiated surface, the change  $LVRPA/I_0$  with respect to  $x$  is linked to extinction coefficients; a rise in catalyst concentration and high extinction coefficients quickly extinguish the total energy of the system. These observations are in good agreement with the literature (Nchikou et al., 2021; Otálvaro-Marín et al., 2014). It is also observed that the more the catalyst loading increases the more the absorption at the reactor bottom decreases. The  $LVRPA/I_0$  is negligible at the reactor bottom for  $C_{cat}$  greater than 0.3 g/L for Catalyst A and Catalyst D, the same result was found by using

the SFM (Otálvaro-Marín et al., 2014) which was validated by comparing it to rigorous solution of

the RTE (Brandi et al., 1999; Zalazar et al., 2005).

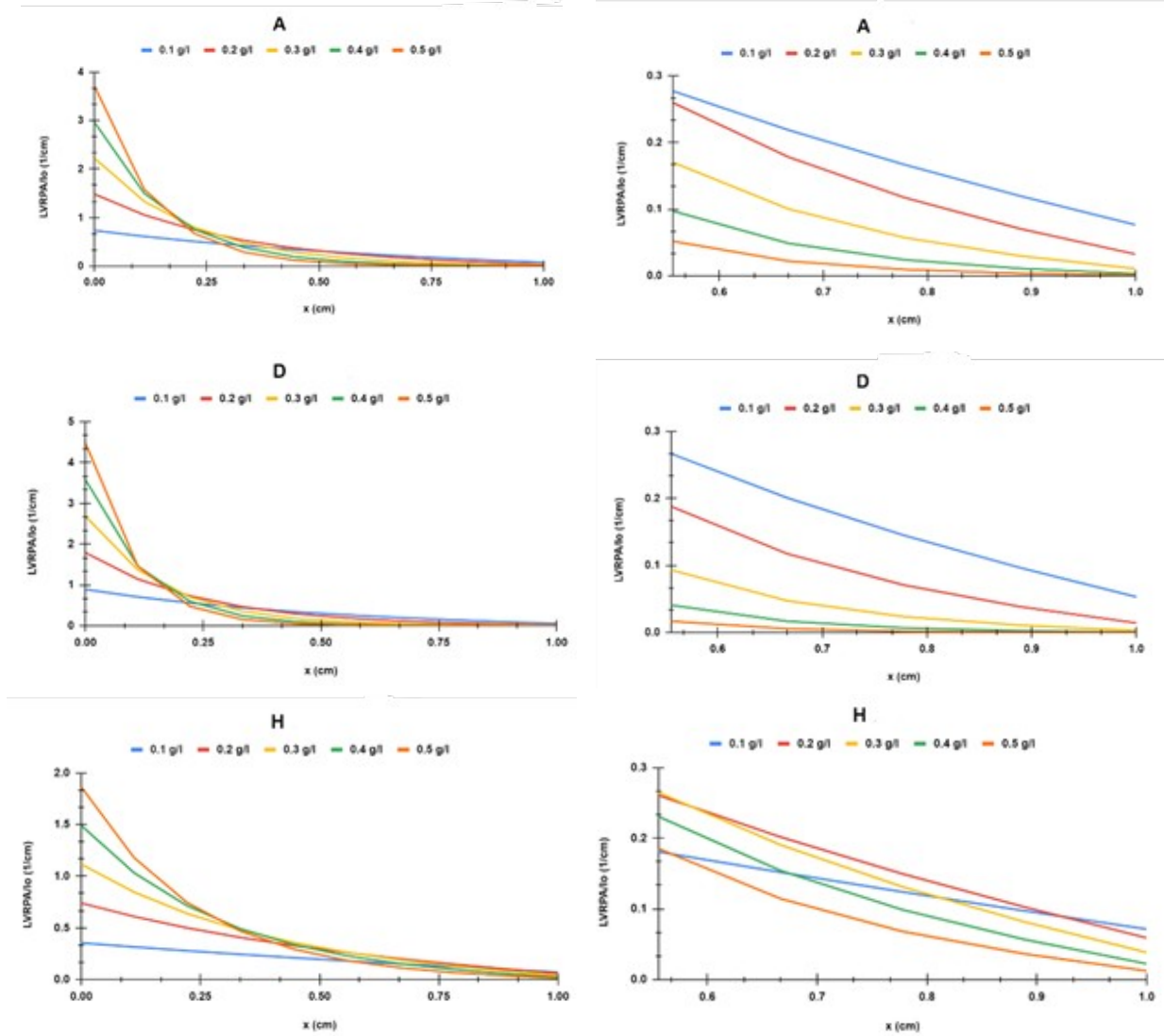


**Figure 2.** The  $LVRPA$  per unit of light intensity vs x-axis with different  $C_{cat}$ , ( $L=1$  cm)  
 a) Catalyst A , b) Catalyst D, c) Catalyst H

The  $LVRPA/I_0$  profile for each catalyst in Figure 3 shows a good uniformization of photon absorption for  $C_{cat}$  equal to 0.1 g/L (Figure 3 a, c, and e) but at 0.5 g/L (Figure 3 b, d, and f) of  $C_{cat}$  photon absorption decreases considerably at the inner zone of the reactor while increases significantly at the

zone around its wall. This could be explained by the fact that the cloudy effect starts which impedes the photon penetration in the inner part of the reactor due to the saturation of the absorption at the irradiated reactor surface (Colina-Márquez et al., 2010). With Catalyst H the clouding effect starts with  $C_{cat}$  greater than 0.5 g/L.

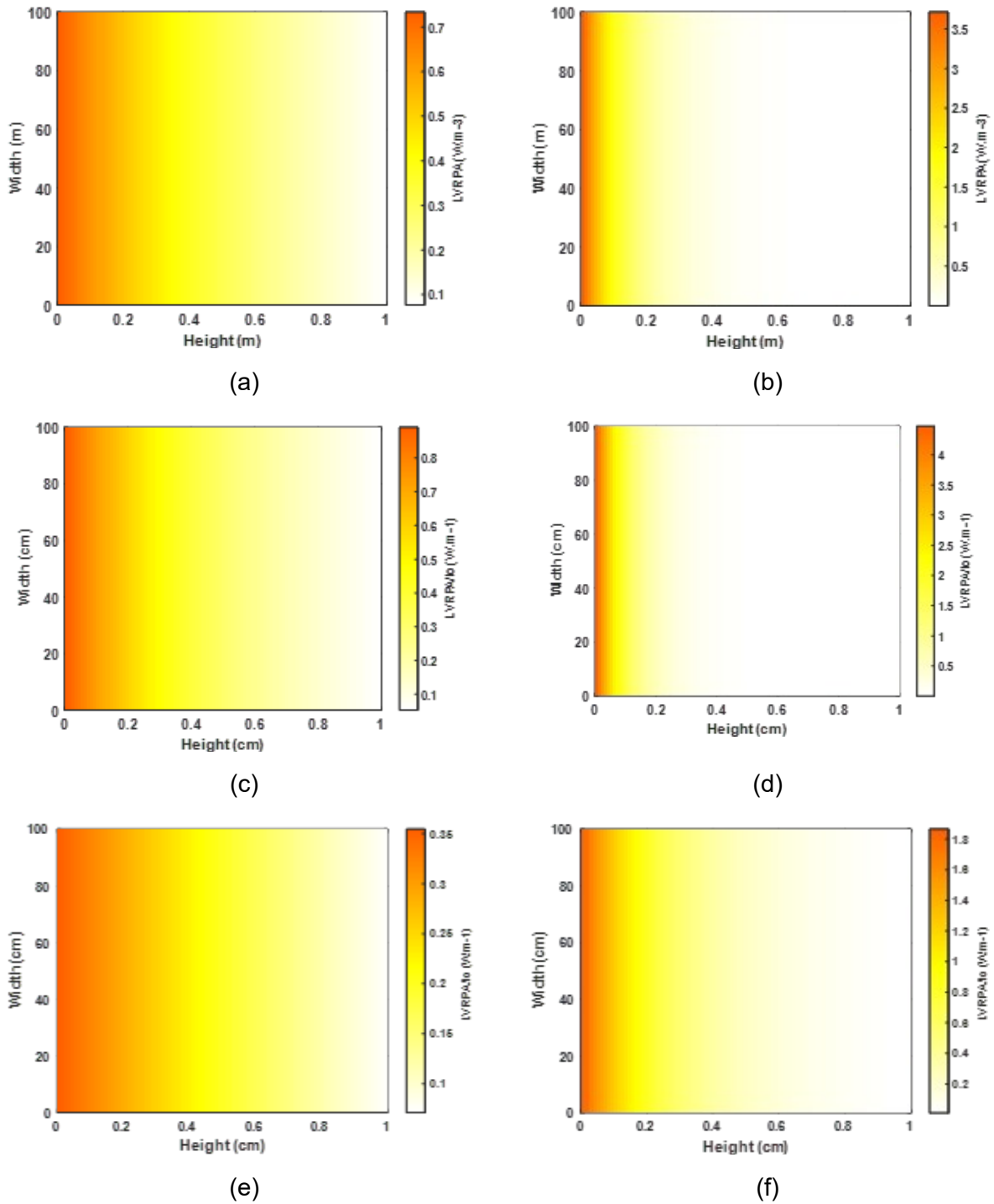


**Figure 3.** Absorption profile per unit of light intensity at 0.1 g/L of  $C_{cat}$  ( a), c), e) for Catalyst A, Catalyst D, and Catalyst H respectively) and at 0.5 g/L of  $C_{cat}$  ( b), d), f) for Catalyst A, Catalyst D, and Catalyst H respectively).

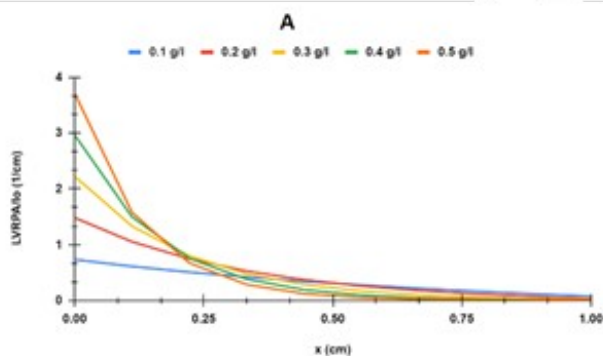
### 3. 2. Optimal Operating Conditions in a Flat Plate Photoreactor

#### 3. 2. 1. VRPA

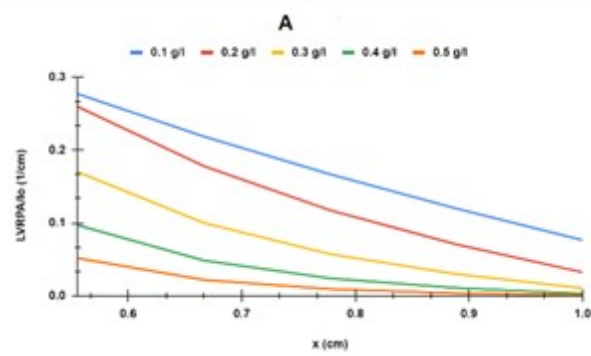
Based on the quantity of radiation absorbed by the catalyst, the  $VRPA$  is crucial for assessing the quantum yield of photocatalytic reactions, it gives more significant information compared to the quantum efficiency, which depends on the incident photon flux. Additionally, it enables a suitable assessment of the activity of catalysts with various optical characteristics (Colina-Márquez et al., 2010). Figure 4 represents the  $VRPA$  per unit of light intensity ( $VRPA/I_0$ ) as a function of catalyst loading with different reactor depths for the three catalysts and different reactor heights. It shows how the  $VRPA/I_0$  increases exponentially and reaches a value from where it remains almost constant due to the photon saturation at the upper side of the reactor. The  $VRPA/I_0$  with Catalyst D is a little higher than with Catalyst A for  $C_{cat}$  less than 0.15 g/L approximately for  $L=0.5\text{ cm}$  and  $L=1\text{ cm}$  but above this value, the reverse is observed. For reactor height higher than unity, Catalyst A has the highest  $VRPA/I_0$  (see Figure 4 a) and b)); meanwhile Catalyst H has the lowest  $VRPA/I_0$  for  $C_{cat}$  less than 0.25 g/L and

almost coincides with Catalyst D in terms of absorption for  $C_{cat}$  greater than 0.25 g/L (see Figure 4 c) and d)).

In the case when  $L=1\text{ cm}$ , the  $VRPA/I_0$  profiles present a weak absorption for  $C_{cat}$  less than 0.1 g/L and from 0.1 to 0.4 g/L an exponential increase; catalyst loading above 0.2, 0.3 and 0.4 g/L respectively for Catalyst D, Catalyst A and Catalyst H would be a catalyst waste since the  $VRPA/I_0$  will no more increase significantly and high value of  $C_{cat}$  produces the clouding effect. The optimum values of  $C_{cat}$  are around 0.2, 0.3, and 0.4 g/L for Catalyst D, Catalyst A, and Catalyst H, respectively, which agree with the literature (Otálvaro-Marín et al., 2014). In comparison to the catalyst Catalyst D, the catalyst Catalyst A  $VRPA$  maximum is approximately 12 % higher. A comparable pattern was observed, where Catalyst A is 19 % and 7 % more efficient than Catalyst D P-25 in the case of UV lamps used for polychromatic radiation and in the case of solar radiation using the SFM approach respectively (Brandi et al., 1999; Otálvaro-Marín et al., 2014). As it is shown in Figure 4, although the  $VRPA/I_0$  increases with  $C_{cat}$ , it decreases with the increase of the reactor height. It drops to 80% approximately for each of the photocatalysts for reactor height varying from 0.5 to 3 cm.



(a)



(b)

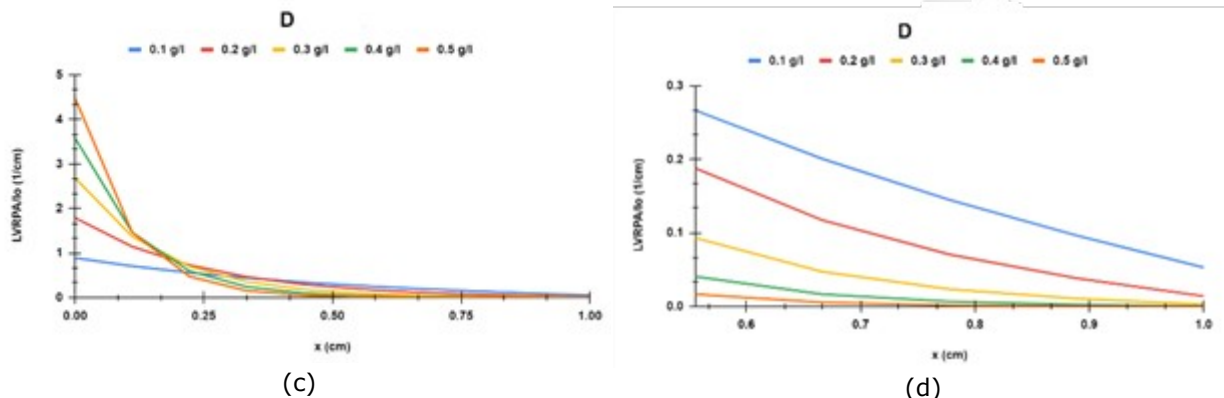
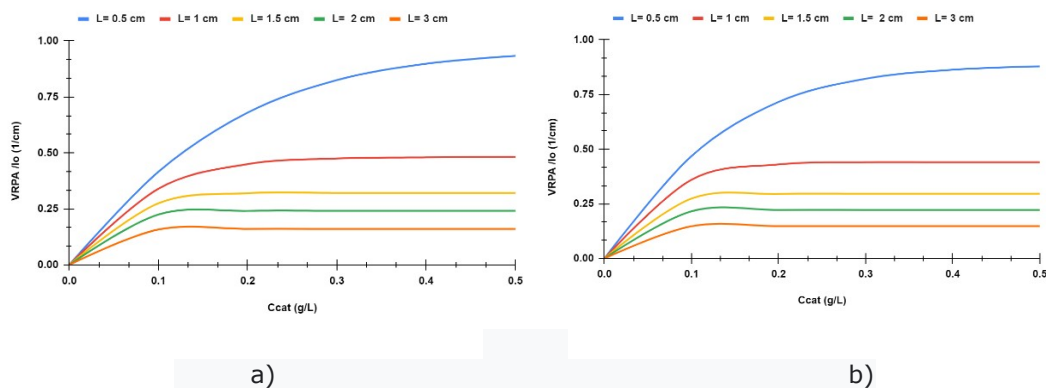


**Figure 4.** The  $VRPA$  per unit of light intensity vs catalyst loading with different reactor depths for the three catalysts (a)  $L=0.5$  cm, b)  $L=1$  cm, c)  $L=2$  cm, d)  $L=3$  cm).

### 3. 2. 2. Impact of the reactor height on the $VRPA$

Figure 5 shows how the reactor height affects the  $VRPA/I_0$  for the three catalysts. In this figure, the  $VRPA/I_0$  decreases with the increase of the reactor height for each of the three catalysts. For both catalysts Catalyst A and Catalyst D, the  $VRPA$  maximum ( $VRPA_{max}/I_0$ ) is reduced to 50% when  $L$  increases from 0.5 to 1 cm and to 30% when  $L$  increases from 1 to 1.5 cm; over 2 cm the  $VRPA_{max}/I_0$  does not vary too much. The same observation is made with the catalyst Catalyst H except that the  $VRPA_{max}/I_0$  decreases to 40 % approximately when increasing  $L$  from 0.5 to 1 cm. These reductions

of the  $VRPA_{max}/I_0$  could be explained by the fact that the more the reactor height increases the more the photon absorption uniformization decreases since the photon pathway becomes very long and it struggles to reach the inner part of the reactor. Moreover, for the catalysts Catalyst A and Catalyst D the optimum  $C_{cat}$  is about 0.15 g/L for  $L > 1$  cm; meanwhile for Catalyst H, the optimum  $C_{cat}$  is about 0.15 g/L for  $L \geq 3$  cm. Thus, for high values of  $L$ , the optimum  $C_{cat}$  is very low but unfortunately working with a very small amount of  $C_{cat}$  implies low production of oxidizing species. Then oversizing the reactor height reduces considerably the average value of the  $LVRPA$  inside the reactor and therefore could disfavor the photocatalytic process.



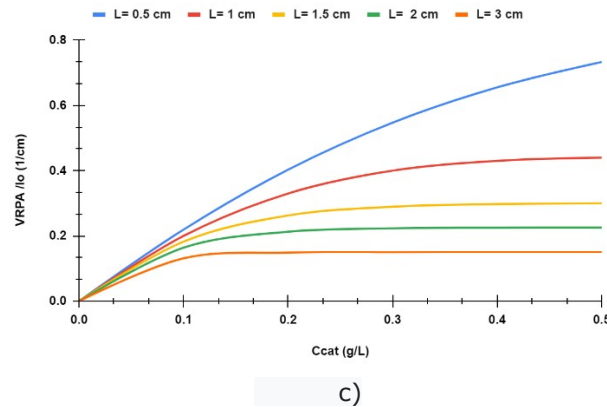


**Figure 5.** The  $VRPA$  per unit of light intensity vs catalyst loading with different reactor depths,  $L = 0.5$  cm in blue line,  $L = 1$  cm in red line,  $L = 1.5$  cm in yellow line,  $L = 2$  cm in green line,  $L = 3$  cm in orange line  
 a) Catalyst A , b) Catalyst D, c) Catalyst H

**4. REACTOR SIZING**

**4. 1. Boundary Layer**

Eq. (28) establishes the boundary layer of photon absorption ( $\delta_{abs}$ ) dependence on the catalyst, catalyst loading, and the reactor thickness. Figure 6 shows how varies  $\delta_{abs}$  with respect to  $C_{cat}$  and  $L$  for the catalysts Catalyst A, Catalyst D and Catalyst H. For any value of  $L$ ,  $\delta_{abs}$  decreases with the increase of  $C_{cat}$  since the more  $C_{cat}$  increases the more photons penetration to the inner part of the reactor becomes difficult. For low values of  $C_{cat}$ ,  $\delta_{abs}$  increases linearly with

$L$ , probably because low  $C_{cat}$  means no saturation of catalyst particles, and therefore, photons can easily move and reach the reactor bottom and then be absorbed ( $\delta_{abs}$  is almost equal to  $L$ ). It is worth mentioning that the more the boundary layer approaches the reactor height the more the absorption is uniform inside the reactor. Finally, for high values of  $C_{cat}$  (greater than 0.5 g/L approximately),  $\delta_{abs}$  increases linearly with  $L$  until a fixed value where it remains almost constant. This is obvious since in this case, the clouding effect occurs because of the presence of a high amount of catalyst particles at the reactor wall impeding photons penetration.

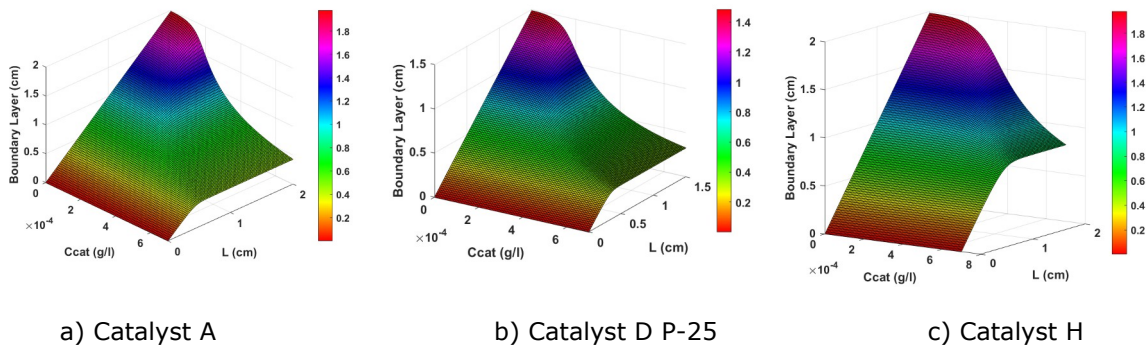


**Figure 6.** Boundary layer of photon absorption as a function of catalyst loading and reactor height for the three catalysts.

Figure 7 shows how the boundary layer of photon absorption varies as a function of catalyst loading ( $L = 1$  cm). Combining Figures 4 and 7 one can find helpful details to specify the kind and amount of catalyst as well as the design thickness of a flat plate reactor. For each of the catalysts, for  $C_{cat}$  lower than 0.1 g/L, absorption takes place in almost the whole reactor but a very small value of the  $VRPA$  is produced ( $\delta_{abs}$  is almost equal to  $L$ ). For  $C_{cat}$  from 0.1 to 0.2 g/L, photon absorption occurs over 85% of the entire reactor height while in the range 0.2-0.4 g/L of  $C_{cat}$ , the  $VRPA$  maximum is obtained between 82 and 89% of the entire reactor thickness as shown in Table 2. This table summarizes the optimum catalyst loading, maximum energy absorbed, and design thickness

for different reactor thicknesses (0.5, 1, 2, and 3 cm). Comparisons have been made between the three catalysts in the literature using the SFM when  $L = 1$  cm (Otálvaro-Marín et al., 2014), and the same observations were found here. As shown in Table 2, Catalyst D is the best catalyst since it needs only 0.2 g/L of  $C_{cat}$  to produce 0.43 (1/cm) of  $VRPA/I_0$  over 86 % of the reactor thickness. It was also found in the literature that for a reactor height of 1 cm, the boundary layer of photon absorption is around 0.86 cm using different Catalyst D optical properties than those in this work (Acosta-Herazo et al., n. d.). Catalyst H comes in third position, it needs 0.4 g/L of  $C_{cat}$  to reach 0.43 (1/cm) of  $VRPA/I_0$  even though it has the highest  $\delta_{abs}$  (0.89). For reactor thickness equal to 0.5 cm, Catalyst A stands as the best photocatalyst and then Catalyst D.

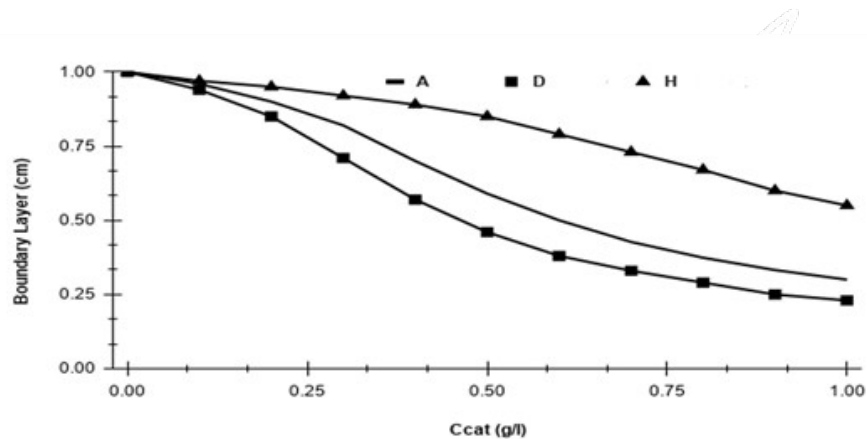


**Figure 7.** Boundary layer of photon absorption as a function of catalyst loading ( $L = 1$  cm).

For  $L = 3$  cm, all the catalysts produce almost the same  $VRPA/I_0$  at the same optimum  $C_{cat}$  (0.15 g/L) but Catalyst H performs as the best

catalyst followed by Catalyst A since Catalyst H has the highest  $\delta_{abs}$  (2.61 cm) and Catalyst D the lowest (1.52 cm).

**Table 2.** Optimum catalyst loading, maximum energy absorbed, and design thickness of flat plate reactor under solar radiation for different reactor heights (0.5, 1, 2, and 3 cm). The values in bracket in column 4 represent  $\frac{\delta_{abs}}{L} \times 100$ .

catalyst	$C_{cat-op}$ (g/L)	$VRPA_{max}/I_0$ (1/cm)	Suggested thickness (cm)	Reactor height (cm)
Catalyst D	0.5	0.88	0.4 (80%)	0.5
	0.2	0.43	0.86 (86%)	1
	0.15	0.22	1.43 (72%)	2
	0.15	0.15	1.52 (51%)	3
Catalyst A	0.5	0.93	0.43 (86%)	0.5
	0.3	0.48	0.82 (82%)	1
	0.15	0.24	1.64 (82%)	2
	0.15	0.16	1.94 (65%)	3
Catalyst H	0.5	0.73	0.47 (94%)	0.5
	0.4	0.43	0.89 (89%)	1
	0.25	0.2	1.85 (93%)	2
	0.15	0.14	2.61 (87%)	3

#### 4. 2. Apparent Optical Thickness

The volumetric rate of photon absorption per unit of reactor length  $VRPA/H$  is another design parameter, it is obtained by integrating the  $LVRPA$  over the reactor width and height. It can also be found by multiplying the  $VRPA$  by the cross-sectional area of the reactor. In this work, the reactor width was supposed to be unity. For the optimization of the radiation absorption inside the flat plate reactor of any height, a new apparent optical thickness  $\zeta_{app1}$  was introduced with the P1 approximation (see Eq. 24) as it was the case of  $\zeta_{app}$  with the SFM approach in the literature (Colina-Márquez et al., 2010). This dimensionless design parameter removes the dependence of the optimum catalyst loading on the reactor height and catalyst albedo as it is proved in Figure 8. Figure 8 a) shows how the  $VRPA/H$  per unit of light intensity ( $\mu\text{mol photons m}^{-2}\text{s}^{-1}$ ) varies as a function of  $\zeta_{app1}$  for different reactor heights with Catalyst D P25 catalyst properties taken from (Colina-Márquez et al., 2010). The optimum value of  $\zeta_{app1}$  ( $\zeta_{app1,op}$ ) remains almost the same (about 4.87) no matter the change in the reactor height. Figure 8 b) displays the variation

of the  $VRPA/H$  as a function of  $\zeta_{app1}$  at different catalyst albedo but with a fixed absorption coefficient ( $\kappa = 2.87 \text{ cm}^2 \text{ g}^{-1}$ ) and  $L=2$  cm. It was found almost the same  $\zeta_{app1,op}$  for different albedo, about 4.87.  $\zeta_{app1}$  keeps the same concept as the  $\zeta_{app}$  with the SFM approach, therefore, reactors working at the same  $\zeta_{app1,op}$  have the same behavior in terms of radiation absorption (Colina-Márquez et al., 2010; Otálvaro-Marín et al., 2014). To prove this affirmation, it was supposed a flat plate reactor working at  $\zeta_{app1,op} = 4.87$  with 0.3 g/L of optimum  $C_{cat}$  and with  $\omega=0.85$ . In this case, the reactor height was found about 1.37 cm using Eq. (24). The corresponding  $VRPA/H$  was established and for comparison purposes, its curve (curve in yellow in Figure 8 b) was drawn as a function of  $\zeta_{app1}$  by taking  $\omega=0.85$  and  $\kappa = 2.87 \text{ cm}^2 \text{ g}^{-1}$  and it was found that it matches the curve in black (see Figure 8 b)  $\omega=0.85$ ). This proves the independence of the optimum catalyst loading on the reactor height and catalyst albedo.  $\zeta_{app1,op}$  values obtained were 4.62, 4.87, and 3.7 for Catalyst A, Catalyst D, and Catalyst H,

respectively, almost the same values of the optimum  $\zeta_{app}$  obtained (4.39, 4.08, and 3.77) with reactor height taken 1 cm by using the features displayed in Table 1. The best design conditions for different catalyst loadings and reactor thicknesses are obtained by keeping

$\zeta_{app1,op}$  constant. For optimization purposes, it is recommended to use  $\zeta_{app}$  when the reactor height is not near 1 cm, therefore, the same recommendation should be considered when using  $\zeta_{app1}$ .

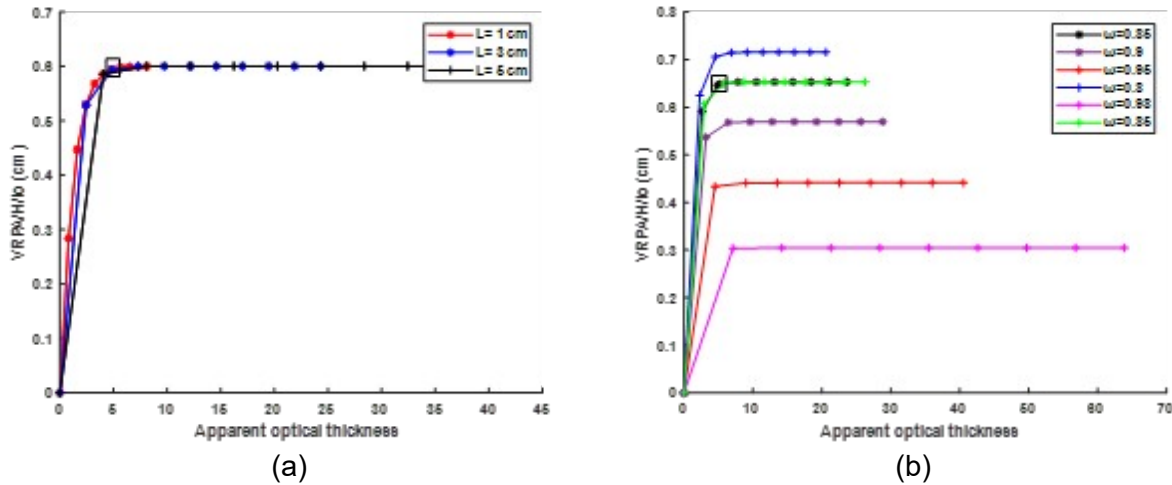


**Figure 8.** a) Effect of the apparent optical thicknesses  $\zeta_{app1}$  on the  $VRPA/H$  per unit of reactor length and per unit of light intensity with a fixed scattering albedo of the photocatalyst at three different reactor heights. Catalyst D P25 catalyst properties were taken from (Colina-Márquez et al., 2010) ( $\omega=0.88$  and  $\kappa=1.74 \text{ cm}^2 \text{ g}^{-1}$ ). The boxed point in the figure corresponds to  $\zeta_{app1,op} = 4.87$  and  $= 0.595 \text{ cm}$ . b) Effect of the apparent optical thicknesses  $\zeta_{app1}$  on the  $VRPA/H$  per unit of reactor length and unit of light intensity as a function of the scattering albedo of the photocatalyst. The specific mass absorption coefficient was kept constant ( $2.87 \text{ cm}^2 \text{ g}^{-1}$ ), and  $\omega$  was varied, with reactor height equal to 2 cm. The yellow line refers to data of the VRPA obtained using  $\zeta_{app1,op} = 4.87$  (the reactor height was found about 1.37 cm using Eq. (24)),  $\omega=0.85$  and  $\kappa=2.87 \text{ cm}^2 \text{ g}^{-1}$ . The boxed point in the figure corresponds to  $\zeta_{app1,op} = 4.87$  and  $= 0.653 \text{ cm}$ .

### 5. PERSPECTIVES

In future works, our attention will be focusing on extending this present work to flat plate photocatalytic reactors with incident radiation varying along the reactor width and this will imply solving the RTE in 2D using the P1 approximation.

### 6. CONCLUSION

In this study, it was demonstrated that the P1 approximation is a viable alternative approach for

characterizing the radiant field in a flat plate reactor with any kind of catalyst present in a high-scattering medium. The radiant field in a flat plate photocatalytic reactor was described and optimized using it. The  $VRPA$ , the boundary layer of photon absorption, and the new apparent optical thickness were established for optimization purposes. These design parameters were used to find the optimum operating conditions employing the catalysts Catalyst D, Catalyst A, and Catalyst H, and comparisons were made between the three catalysts as well.

While the new apparent optical thickness established with the P1 approximation approach eliminates the dependence of the optimum catalyst loading on the reactor height and catalyst albedo, the *VRPA* and the boundary layer of photon absorption help determine the optimal catalyst loading for any reactor height and reactor sizing, respectively. Findings are consistent with those obtained using the SFM and could help for scaling up. The significance of the information provided here for flat plate photoreactor design resides in its ability to remove the necessity for statistical analysis of experimental designs, which requires a major investment of time and resources. Establishing a rate equation to explain the kinetics of the photocatalytic degradation of different chemicals could also benefit from this.

## 7. ACKNOWLEDGMENTS

Dr. Clovis Nchikou dedicates this article to the memory of Dr. Juan-Antonio Rojas-Estrada.

## 8. COMPETING INTERESTS

The author declares that he has no known competing financial interests or personal relationships that could have appeared to influence the work reported in this article.

## 9. REFERENCES

Acosta-Herazo, R., Cañaverel-Velásquez, B., Pérez-Giraldo, K., Mueses, M. A., Pinzón-Cárdenas, M. H., & Machuca-Martínez, F. (2020). A MATLAB-Based Application for Modeling and Simulation of Solar Slurry Photocatalytic Reactors for Environmental Applications. *Water*, *12*(8), 2196. <https://doi.org/10.3390/w12082196>

Acosta-Herazo, R., Monterroza-Romero, J., Mueses, M. Á., Machuca-Martínez, F., & Li Puma, G. (2016). Coupling the Six Flux Absorption-Scattering Model to the Henyey-Greenstein scattering phase function: Evaluation and optimization of radiation absorption in solar heterogeneous photoreactors. *Chemical Engineering Journal*, *302*, 86-96. <https://doi.org/10.1016/j.cej.2016.04.127>

Acosta-Herazo, R., Mueses, M. Á., Machuca-Martínez, F., & Li, G. (s. f.). *Layer of photon absorption and apparent optical thickness*.

Akdemir, O., Lagendijk, A., & Vos, W. L. (2022). Breakdown of light transport models in photonic scattering slabs with strong absorption and anisotropy. *Physical Review A*, *105*(3), 033517. <https://doi.org/10.1103/PhysRevA.105.033517>

Arancibia-Bulnes, C. A., Jiménez, A. E., & Estrada, C. A. (2009). Development and Modeling of Solar Photocatalytic Reactors. En *Advances in Chemical Engineering* (Vol. 36, pp. 185-227). Elsevier. [https://doi.org/10.1016/S0065-2377\(09\)00406-2](https://doi.org/10.1016/S0065-2377(09)00406-2)

Brandi, R. J., Alfano, O. M., & Cassano, A. E. (1996). Modeling of radiation absorption in a flat plate photocatalytic reactor. *Chemical Engineering Science*, *51*(11), 3169-3174. [https://doi.org/10.1016/0009-2509\(96\)00215-1](https://doi.org/10.1016/0009-2509(96)00215-1)

Brandi, R. J., Alfano, O. M., & Cassano, A. E. (1999). Rigorous model and experimental verification of the radiation field in a flat-plate solar collector simulator employed for photocatalytic reactions. *Chemical Engineering Science*.

Cassano, A. E., Martin, C. A., Brandi, R. J., & Alfano, O. M. (1995). Photoreactor Analysis and Design: Fundamentals and Applications. *Industrial & Engineering Chemistry Research*, *34*(7), 2155-2201. <https://doi.org/10.1021/ie00046a001>

Christenson, J. G., Austin, R. A., & Phillips, R. J. (2018). Comparison of approximate solutions to the phonon Boltzmann transport equation with the relaxation time approximation: Spherical harmonics expansions and the discrete ordinates method. *Journal of Applied Physics*, *123*(17), 174304. <https://doi.org/10.1063/1.5022182>

Colina-Márquez, J., Machuca-Martínez, F., & Li Puma, G. (2015). Modeling the Photocatalytic Mineralization in Water of Commercial Formulation of Estrogens 17- $\beta$  Estradiol (E2) and Noregestrol Acetate in Contraceptive Pills in a Solar Powered Compound Parabolic Collector. *Molecules*, *20*(7), 13354-13373. <https://doi.org/10.3390/molecules200713354>

Colina-Márquez, J., Machuca-Martínez, F., & Puma, G. L. (2010). Radiation Absorption and Optimization of Solar Photocatalytic Reactors for Environmental Applications. *Environmental Science & Technology*, *44*(13), 5112-5120. <https://doi.org/10.1021/es100130h>

Cuevas, S. A., & Arancibia-Bulnes, C. A. (s. f.). *Modeling UV radiation absorption in a flat-plate photocatalytic reactor*.

Cuevas, S. A., Arancibia-Bulnes, C. A., & Serrano, B. (2007). Radiation Field in an Annular

- Photocatalytic Reactor by the P1 Approximation. *International Journal of Chemical Reactor Engineering*, 5(1). <https://doi.org/10.2202/1542-6580.1589>
- Fujii, H., Terabayashi, I., Aoki, T., Inoue, Y., Na, H., Kobayashi, K., & Watanabe, M. (2022). Numerical Study of Near-Infrared Light Propagation in Aqueous Alumina Suspensions Using the Steady-State Radiative Transfer Equation and Dependent Scattering Theory. *Applied Sciences*, 12(3), 1190. <https://doi.org/10.3390/app12031190>
- Ghafoori, S., Nasirian, M., Al-Jamal, R., Mallouh, F. A., & Mehrvar, M. (2020). Statistical parameter optimization and modeling of photodegradation of methyl orange using a composite photocatalyst prepared by thermal synthesis. *Environmental Science and Pollution Research*, 27(36), 45650-45660. <https://doi.org/10.1007/s11356-020-10301-5>
- Harel, R., Burov, S., & Heizler, S. I. (2021). Asymptotic  $P_N$  Approximation in Radiative Transfer Problems. *Journal of Computational and Theoretical Transport*, 50(5), 390-406. <https://doi.org/10.1080/23324309.2020.1845738>
- He, C., Clifton, O., Felker-Quinn, E., Fulgham, S. R., Juncosa Calahorrano, J. F., Lombardozzi, D., Purser, G., Riches, M., Schwantes, R., Tang, W., Poulter, B., & Steiner, A. L. (2021). Interactions between Air Pollution and Terrestrial Ecosystems: Perspectives on Challenges and Future Directions. *Bulletin of the American Meteorological Society*, 102(3), E525-E538. <https://doi.org/10.1175/BAMS-D-20-0066.1>
- Howell, J. R., Mengüç, M. P., Daun, K. J., & Siegel, R. (2021). *Thermal radiation heat transfer* (Seventh edition). CRC Press.
- Illi, E., Bouanani, F. E., Park, K.-H., Ayoub, F., & Alouini, M.-S. (2019). An Improved Accurate Solver for the Time-Dependent RTE in Underwater Optical Wireless Communications. *IEEE Access*, 7, 96478-96494. <https://doi.org/10.1109/ACCESS.2019.2929122>
- Incropera, F. P. (s. f.). [PDF] *Fundamentals Of Heat And Mass Transfer*.
- Li, J., Carlson, B. E., Yung, Y. L., Lv, D., Hansen, J., Penner, J. E., Liao, H., Ramaswamy, V., Kahn, R. A., Zhang, P., Dubovik, O., Ding, A., Lacis, A. A., Zhang, L., & Dong, Y. (2022). Scattering and absorbing aerosols in the climate system. *Nature Reviews Earth & Environment*, 3(6), 363-379. <https://doi.org/10.1038/s43017-022-00296-7>
- Li Puma, G. (2005). Dimensionless Analysis of Photocatalytic Reactors Using Suspended Solid Photocatalysts. *Chemical Engineering Research and Design*, 83(7), 820-826. <https://doi.org/10.1205/cherd.04336>
- Li Puma, G., Machuca-Martínez, F., Mueses, M., Colina-Márquez, J., & Bustillo-Lecompte, C. (2020). Scale-Up and Optimization for Slurry Photoreactors. En C. Bustillo-Lecompte (Ed.), *Advanced Oxidation Processes—Applications, Trends, and Prospects*. IntechOpen. <https://doi.org/10.5772/intechopen.91920>
- Moreno-SanSegundo, J., Casado, C., & Marugán, J. (2020). Enhanced numerical simulation of photocatalytic reactors with an improved solver for the radiative transfer equation. *Chemical Engineering Journal*, 388, 124183. <https://doi.org/10.1016/j.cej.2020.124183>
- Nair, A. K., & JagadeeshBabu, P. E. (2017). Ag-TiO<sub>2</sub> nanosheet embedded photocatalytic membrane for solar water treatment. *Journal of Environmental Chemical Engineering*, 5(4), 4128-4133. <https://doi.org/10.1016/j.jece.2017.07.046>
- Nchikou, C., Loredó-Medrano, J. Á., Hernández-Ramírez, A., Colina-Marquez, J. Á., & Mueses, M. Á. (2021). Estimation of the radiation field for CPC photocatalytic reactors using a novel six-flux model in two dimensions (SFM-2D). *Journal of Environmental Chemical Engineering*, 9(6), 106392. <https://doi.org/10.1016/j.jece.2021.106392>
- Ochoa-Gutiérrez, K. S., Tabares-Aguilar, E., Mueses, M. Á., Machuca-Martínez, F., & Li Puma, G. (2018). A Novel Prototype Offset Multi Tubular Photoreactor (OMTP) for solar photocatalytic degradation of water contaminants. *Chemical Engineering Journal*, 341, 628-638. <https://doi.org/10.1016/j.cej.2018.02.068>
- Otálvaro-Marín, H. L., Mueses, M. A., & Machuca-Martínez, F. (2014). Boundary Layer of Photon Absorption Applied to Heterogeneous Photocatalytic Solar Flat Plate Reactor Design. *International Journal of Photoenergy*, 2014, 1-8. <https://doi.org/10.1155/2014/930439>
- Peralta Muniz Moreira, R., & Li Puma, G. (2021). Multiphysics Computational Fluid-Dynamics (CFD) Modeling of Annular Photocatalytic Reactors by the Discrete Ordinates Method (DOM) and the Six-Flux Model (SFM) and Evaluation of the Contaminant Intrinsic Kinetics Constants. *Catalysis Today*, 361, 77-84. <https://doi.org/10.1016/j.cattod.2020.01.012>

- Rizzo, L., Malato, S., Antakyali, D., Beretsou, V. G., Đolić, M. B., Gernjak, W., Heath, E., Ivancev-Tumbas, I., Karaolia, P., Lado Ribeiro, A. R., Mascolo, G., McArdeall, C. S., Schaar, H., Silva, A. M. T., & Fatta-Kassinos, D. (2019). Consolidated vs new advanced treatment methods for the removal of contaminants of emerging concern from urban wastewater. *Science of The Total Environment*, 655, 986-1008. <https://doi.org/10.1016/j.scitotenv.2018.11.265>
- Tourasse, G., & Dumortier, D. (2014). Development of a System Measuring the Solar Radiation Spectrum in 5 Planes for Daylight and PV Applications. *Energy Procedia*, 57, 1110-1119. <https://doi.org/10.1016/j.egypro.2014.10.071>
- Vaya, D., & Surolia, P. K. (2020). Semiconductor based photocatalytic degradation of pesticides: An overview. *Environmental Technology & Innovation*, 20, 101128. <https://doi.org/10.1016/j.eti.2020.101128>
- Wang, D., Mueses, M. A., Márquez, J. A. C., Machuca-Martínez, F., Grčić, I., Peralta Muniz Moreira, R., & Li Puma, G. (2021). Engineering and modeling perspectives on photocatalytic reactors for water treatment. *Water Research*, 202, 117421. <https://doi.org/10.1016/j.watres.2021.117421>
- Zalazar, C. S., Romero, R. L., Martín, C. A., & Cassano, A. E. (2005). Photocatalytic intrinsic reaction kinetics I: Mineralization of dichloroacetic acid. *Chemical Engineering Science*, 60(19), 5240-5254. <https://doi.org/10.1016/j.ces.2005.04.050>